Well integrity assessment by a 1:1 scale wellbore experiment: Exposition to dissolved CO2 and overcoring

Jean-Charles Manceau, Joachim Tremosa, Catherine Lerouge, F. Gherardi, C. Nussbaum, L.J. Wasch, Patrick Albéric, Pascal Audigane, Francis Claret

HAL Id: insu-01374252
https://insu.hal.science/insu-01374252

Submitted on 12 Dec 2016

Well integrity assessment by a 1:1 scale wellbore experiment: Exposition to dissolved CO$_2$ and overcoring

J.C. Manceau, J. Tremosa, C. Lerouge, F. Gherardi, C. Nussbaum, L.J. Wasch, P. Alberic, P. Audigane, F. Claret

Highlights

• A 1:1 scale experiment on well integrity is carried out in a rock laboratory.

• The stage B dedicated to well exposure to CO$_2$-rich pore water is presented.

• The well system has been ultimately overcored for inspection.

• Key messages on processes affecting the integrity of a well are derived.

• Similar experimental set-up could be used for other aspects of well integrity.

Abstract

In this work, we present the results of a new in situ experiment to complete the existing scientific dataset on well integrity in the context of CO$_2$ storage. This experimentation has been designed to evaluate the sealing behaviour of a monitored well after mechanical and chemical stresses due to pressure and temperature changes (*stage A*) and due to the exposure to carbonated brine (*stage B*), before a final overcoring stage for retrieving the well system and the surrounding clay. The *stage A* has been the subject of a first publication (Manceau et al., 2015; Water Resour. Res., 51, 6093–6109) and the two latter stages are described in this paper. Multidisciplinary methods (hydraulic tests and modelling, fluid sampling and modelling, analysis of cement and clay samples on the overcore) are used to get better insight, in a realistic wellbore context, on the interplay between the geochemical questions, and the operational and construction issues. In particular, this study shows that when good integrity pre-exists before a well is in contact with carbonated water, the exposure to dissolved CO$_2$ does not seem to lead to a degradation of the well hydraulic properties but rather to their improvement.

1. Introduction

Achieving good well integrity (i.e. zonal isolation of geologic formations, cf. Crow et al., 2010) requires drillers and operators to follow best practices during borehole drilling, well completion, well operations and abandonment. The existence of an abnormal borehole damaged zone, poor cement mixing, gas or formation fluid migration, difficulties in removing drilling mud and cement shrinkage during curing are some of the construction issues frequently cited in the literature (see e.g. Gasda et al., 2008, Kuperschmied et al., 2015, Zhang and Bachu, 2011, Nelson, 1990, Bonett and Pafitis, 1996 and Choi et al., 2013). The well integrity quality also depends on how the operations that the well is experiencing (both during its active life and after its abandonment) modify the initial wellbore properties. Significant changes in formation- or casing-pressure and/or temperature could damage the near-well formation, the casing or the cement sheath as well as detach the bonding of those elements (Nelson, 1990, Zhang and Bachu, 2011, Carey, 2013, Bai et al., 2015 and Vrålstad et al., 2015). Integrity problems could arise from micro annuli formed due to such mechanical stresses. The wellbore can also be impacted by the geochemical environment in which it has been completed: abnormal caprock and cement degradation as well as casing corrosion may arise in some cases (highly saline and corrosive brine for instance, cf. (Nelson, 1990).

On a geological carbon dioxide storage site, decommissioned wells drilled through low-permeable caprock are potential connections between the CO_2 storage reservoir and overlying sensitive targets like aquifers. In sedimentary basins already used for oil and gas or geothermal resources, such wells are likely to be present in large numbers within the CO_2 storage complex. In addition, materials commonly used for well completion (Portland cement and steel casing) are known to react with the low-pH carbonated brine resulting from the CO_2 injection operations (Bruckdorfer, 1986, Carey, 2013 and Walsh et al., 2014). Those geochemical reactions, and their potential impacts on the creation/increase of flow pathways, have been the subject of the majority of the research effort relative

to well integrity in the field of CO$_2$ storage (see e.g. the review by Carroll et al., (2016)).

Portland cement reactivity after CO$_2$ exposure has been studied by experiments in batch reactors to assess the evolution of the cement intrinsic properties (hydraulic and mechanical) (Barlet-Gouédard et al., 2009; Duguid and Scherer, 2010; Jung and Um, 2013; Kutchko et al., 2007, 2008, 2009; Lesti et al., 2013; Rimmelé et al., 2008). The effect of exposure to wet supercritical CO$_2$ or to CO$_2$-saturated water or brine has been observed with different cement types, and different experimental conditions (fluid composition, water/cement ratio, curing conditions, pressure and temperature). The studies agree on a similar geochemical process (explained for instance in Abdoulghafour et al. (2013)): the diffusion of carbonated brine within the cement first leads to the dissolution of portlandite (calcium hydroxide) and subsequently of calcium silicate hydrate phases (CSH), buffering the low CO$_2$-rich brine pH and producing calcium ions. Together with carbonate species, these ions form calcium carbonate (carbonation). Especially in an advection dominated regime, calcium carbonate can re-dissolve and leave an amorphous silica gel (or amorphous zeolite, cf. Mason et al. (2013)) after the dissolution of the remaining calcium silicate hydrate phases. Three reaction zones are consequently observed after cement exposure to CO$_2$-saturated brine (e.g. Kutchko et al. (2008)): A region depleted in portlandite close to unaltered cement, a zone with calcium carbonate precipitation characterised by an orange colouration and, in contact with the carbonated brine, a silica rich amorphous region. Even though the carbonated zone has been shown to be less permeable and mechanically stronger, the opposite has been measured for the zone enriched in amorphous silica. Given the different conditions at which experiments are undertaken, the results of the existing studies are mixed, but cement alteration does not appear to lead to increase in permeability capable of compromising well integrity (Carey, 2013).

Concerns have been raised about the influence of geochemistry on the flow through existing defects within cement. Works have been performed to assess the behaviour of fractured cement exposed to brine and/or CO$_2$ (Huerta et al., 2013, 2016; Liteanu and Spiers, 2011; Luquot et al., 2013; Walsh et al., 2013; Wigand et al., 2009), as well as of composite materials representing flow pathways along wellbore interfaces (Carey et al. (2010) for the casing/cement interface; Mason et al. (2013) and Walsh et al. (2014) for the caprock/cement interface). Most of these studies observed a decrease of effective absolute permeability of the cement. This could be due to fracture healing by calcium carbonate precipitation (Wigand et al., 2009; Liteanu and Spiers, 2011), due to the development of the very low permeable amorphous silica-rich zone (Abdoulghafour et al., 2013), or due to mechanical degradation of the altered layers leading to a deformation of the fracture/leakage pathway (Mason et al., 2013; Walsh et al., 2014). However, Luquot et al. (2013) showed a more complex behaviour, with a dependence of the fracture permeability notably to the fracture aperture and to renewal rate of the carbonated brine within the fracture.

Steel casing corrosion has also been widely studied in a CO$_2$-free context (the types of corrosion that can be encountered in downhole conditions are for instance described in Talabani et al. (2000)) and in CO$_2$-rich environments (an exhaustive review is given in Choi et al. (2013)). All those studies highlighted the importance of the alkaline environment provided by the cement sheath that protects the casing against corrosion (passivation). They also described dissolved CO$_2$ as a corrosive specie capable of high corrosion rates in case of direct exposure on steel casing (under unfavourable conditions, rates up to 20 mm/year are given in Choi et al. (2013)).

Caprock alteration (close to the cement sheath) is also suspected to play a role in well integrity evolution (Mason et al., 2013). The geochemical reactions involving for instance carbonate-rich or clay-rich caprocks may induce pore-water or mineralogical changes and could play a role in the reactivity of the well close environment and consequently in the changes of hydraulic properties.

The existing research activities in the well integrity domain often conclude on the importance of considering this issue as a multi-physical problem with coupled hydrodynamic, geomechanical and geochemical phenomena. Understanding what could occur realistically in the field is indeed a difficult point, as it implies reproducing in situ conditions. This difficulty has been tackled by combining observations made on industrial CO$_2$ storage analogues with the results of laboratory experiments. For instance, to assess CO$_2$ interactions with the wellbore, samples have been collected from an existing CO$_2$-EOR well (35 years of operations with CO$_2$) (Carey et al., 2007) and from a natural CO$_2$ producer (30 years of production) (Crow et al., 2010). Nevertheless, determining some key properties on real wells is challenging, such as measuring effective permeability (cf. Gasda et al. (2008)), and therefore the comparison between field and laboratory outcomes can only be partial.

In this work, we present the results of a new experiment to fill the gaps in the existing scientific dataset on well integrity in the context of CO$_2$ storage. The innovativeness of this experiment is that the well integrity is assessed accounting for all the components of a well (casing, cement, caprock formation), using common geometry and materials, and with significantly detailed instrumentation to enable access to parameters usually difficult to measure. This experiment has been designed to evaluate the sealing behaviour of a well after mechanical and chemical stresses due to pressure and temperature changes (*stage A*) and due to the exposure to carbonated brine (*stage B*). The *stage A* has been the subject of a first publication (Manceau et al., 2015) and the *stage B* is described in this paper. The paper also presents the outcomes of the overcoring procedure (similar procedures have already been carried out in other contexts, e.g. Koroleva et al. (2011), Jenni et al. (2014)).

The main purpose of this paper is to understand how exposure to CO$_2$-rich brine can affect well integrity in a realistic environment and to get better insight, in this complex context, in the interplay between geochemistry, and the operational and construction issues.

After presenting the experimental design, the results of the first stage are briefly recalled; the protocol of the second stage is explained and the hydraulic and geochemical datasets gathered during the monitoring of the experiment are presented. We interpret these outcomes with dedicated modelling and with additional materials collected and analysed after the overcoring of the well system.

2. Previous operations: design and well integrity assessment under temperature and pressure stresses

In this section, we recap essential information for understanding *stage B*. For an extensive description of the experimental concept and of *stage A*, the reader is referred to Manceau et al. (2015).

2.1. Experimental set-up

The experiment took place in the Opalinus Clay formation (shaly facies) of the Mont Terri Underground Rock Laboratory (St-Ursanne, Canton of Jura, North-Western Switzerland). The Mont Terri Underground Rock Laboratory crosses the Mont Terri anticline formed during the folding of the Jura Mountains in the Late Miocene to Pliocene period, around 10–2 Million years ago. The Opalinus Clay consists mainly of incompetent, silty and sandy shales, deposited around 175 My (Aalenien/Toarcian), buried at least at 1350 m (the present overburden thickness is 300 m) (Bossart and Thury, 2008).
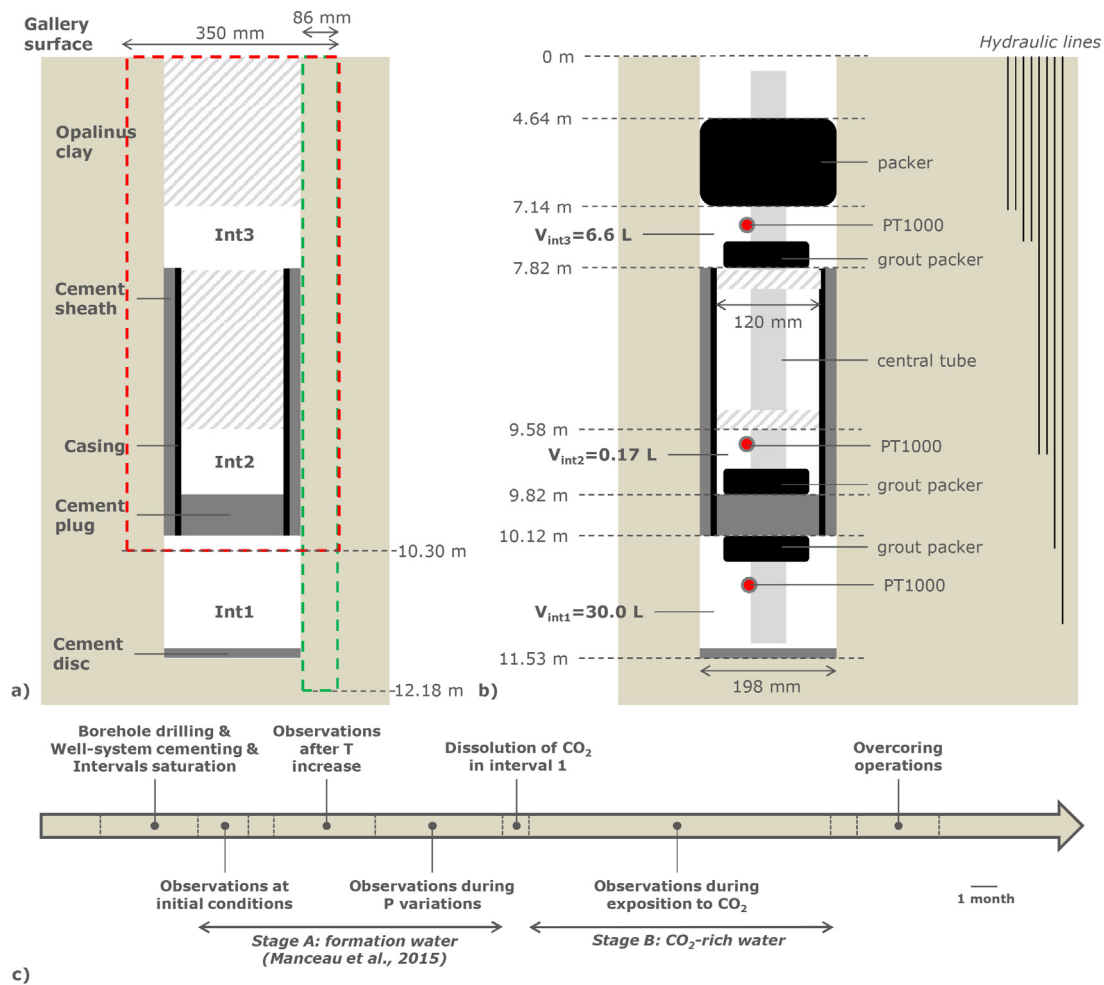
Fig. 1. a) Concept of the experimentation with the sketch of the overcoring operations: in green, contour of borehole BCS-5A; in red, contour of the overcore BCS-5OC (not to scale) b) technical layout of the completion; only the hydraulic lines used for pressure monitoring, fluid extraction and injection are represented (not to scale) c) time-line of the whole experiment. (For interpretation of the references to colour in this figure legend, the reader is referred to the web version of this article.)

Figure modified after Manceau et al. (2015).

This overconsolidated shale formation can be considered as a reference caprock-like formation.

The concept and the technical layout of the experiment are provided in Fig. 1(a and b). A shallow and small section of a wellbore (2.30 m-long and 10.1 m-deep from the laboratory gallery ground level) has been constructed at scale 1:1 (198 mm diameter borehole, and 5.5" casing – outside diameter 160 mm and inside diameter: 140 mm), using a carbon steel casing and class G cement (common oil and gas wells materials). Two different zones of interest have been observed, a first one with the casing internal side and the cement plug, and a second one with the casing external side, the cement annulus/sheath and the formation rock.

With the aim of characterizing these zones, three different intervals (i.e. a volume with no material) have been designed for:

- a continuous monitoring of the pressure and temperature conditions. Temperature is measured with PT1000 probes and pressure is measured with pressure transducers located at the surface control board;
- injecting or extracting fluids to set specific pressure or flux conditions and to sample fluids. The injection of fluids (liquid and gas) is performed with a syringe pump Teledyne Isco (model 500D). The fluids are extracted with a mass flow meter (Bronkhorst Thermal Mass Flow Meter, 0–10 g/h, 1–20 bar). Both the pump and the

flow controller module are remotely controlled with the DCAM software (Solexperts AG).

Interval 1 (ca. 30 L) is located below the well-section, interval 2 (0.17 L) over the cement plug, and interval 3 (6.6 L) over the well-section. Temperature in interval 1 can be controlled by the circulation of boric acid within the central stainless steel tube of interval 1. The cementing of the sheath and the plug has been allowed by a mechanical (grout) packer system. The isolation of the whole system from the surface is insured by a 2.5 m long packer, placed over interval 3. The system GeoMonitor (Solexperts AG) is used for data acquisition.

2.2. Stage A: implementation and outcomes

The borehole drilling stage (October 1st, 2012, a time-line of the whole experimental work is provided on Fig. 1c) has shown a relatively low gallery excavation damaged zone (60 cm). This impacted zone was therefore located much shallower than the well-system depth, and was not likely to interfere with the experiment. The well-system has been installed and cemented on October 4th, 2012. Given that the volumes of the intervals were significant compared to the natural pore water flow in the Opalinus Clay, the three intervals were filled with Pearson water (synthetic pore water rep-

resentative of the native formation water, Pearson et al. (2011)). The artificial saturation stage lasted two months.

The well integrity has been assessed during *stage A* for different conditions. This assessment was performed first at initial conditions (period 1: February–March 2013, ca. 10 bar and 17 °C in interval 1), then after an increase of the well-system temperature (period 2: May–August 2013, ca. 10 bar and 52 °C in interval 1) and after sharp variations in interval 1 pressure (period 3: September 2013–January 2014, 10–30 bar, 31 °C). The effective well permeability was estimated after constant head hydraulic tests (constant head in interval 1) and after circulation steady state tests (injection at constant head in interval 1 and extraction at constant rate in interval 3). Only the effective permeability of the region behind casing has been measured since there was no connection through the cement plug (i.e. between interval 1 and 2). The chemistry of the well system has been characterised after regular sampling in interval 1 and 3.

Important conclusions have been derived from *stage A*:

- The effective well permeability estimated all along *stage A* (between 2×10^{-14} m^2 and 8×10^{-19} m^2) was higher than the cement or caprock permeability. This suggested that preferential flow pathways existed, especially at the very beginning of the experiment when the effective well permeability was at its highest level. The assumption of the presence of pathways was later confirmed by the geochemical evolution of the fluids and by the observation that the effective well permeability depended on pressure. This would mean that the effective well permeability is partly, possibly entirely, due to the flow at the interfaces between the caprock and the cement annulus, supporting the acknowledged importance of the cementing process during well construction.
- The temperature and pressure stresses applied to the well-system during *stage A* appeared to influence significantly the effective well permeability. Increasing temperature decreased the effective well permeability by approximately 3 orders of magnitude, while increasing pressure at the well bottom increased it by more than 2 orders of magnitude. This would indicate that operations-induced stresses could influence the well integrity as much as the cementing process.

3. Exposure of the well-system to CO$_2$-rich pore water (*stage B*) and overcoring operations

3.1. Dissolution of gaseous CO$_2$ within interval 1

Stage B was dedicated to the exposure of the well-system to CO$_2$-rich pore water. The injected CO$_2$ gas had a specific isotopic signature δ^{13}C (+15.8‰ *vs.* PDB[1]), chosen to be significantly different from the isotopic signatures of the carbon reservoirs of the clay formation (carbonates, carbon species dissolved in pore water, organic matter). Bromide, with an expected initial concentration in interval 1 of 1×10^{-3} mol/L (3.087 g of NaBr have been introduced) has also been used as an additional tracer. It has been injected in the injection line just before the starting of the CO$_2$ injection.

The objective was similar to *stage A*, i.e. to force a continuous migration of pore-water from the bottom of the well to the top, but, for that stage, replacing the synthetic water by carbonated water. In order to ensure stable pressure conditions during the formation-water replacement, CO$_2$ in gas phase has been continuously injected at 19 °C and 25 bar during two weeks. This injection has been performed at the bottom of interval 1 to ensure a bub-

bling along the 1.35 m-long interval and a progressive dissolution of the injected CO$_2$. 7560 mL of CO$_2$ gas was injected (see Fig. 2d), corresponding to a mass of 402 g (the densities are computed after Lemmon et al. (2013)).

3.2. Circulation steady state tests with carbonated brine

After March 4, 2014, circulation steady state tests have been carried out similarly as during *stage A* with constant head injection of carbonated brine in interval 1 and extraction at constant rate in interval 3 (Fig. 2). For the continuous injection of carbonated brine, the dissolution of CO$_2$ in synthetic pore water was performed at the surface in a pressure vessel. The dissolution conditions (as constrained by the pressure limitation of the pressure vessel) were during most of *stage B* at approximately 19.5 °C and 14 bar (the pressure was lower between March and May, 2014).

At the beginning, tests were performed with a pressure of 28 bar in interval 1 and an extraction rate of 0.16 g/h in interval 3. The extraction rate has been doubled on April 7th 2014 in order to favour the fluid flow through the well to interval 3. As done during *stage A-period 3*, three pressure increases in interval 1 have been imposed during this period (similar to HI tests, but the extraction rates were maintained during those increases): A +2 bar step on May 19th, a +8 bar step on June 3rd and a +6 bar step on July 10th. The effect of these three increases is visible in the interval 3 pressure evolution but the effect is very small.

3.3. Leakage in interval 3 and continuation of the well exposure to carbonated brine

On August 6th 2014, a loss of integrity in interval 3 occurred, leading to a rapid decrease of the pressure in interval 3, down to values lower than 1 bar (measured at the surface). In order to find the location of the leakage, four N$_2$ injection tests were performed on August 12th, on August 21st, on September 10th and on September 18th. No leakage was detected on surface equipment. During test 4, the central tube of the well completion (which reaches the surface) was investigated. In this central rod, noise of bubbling was heard and dust exhaust was observed at the surface, indicating a leakage coming directly from interval 3, more precisely via a connection between interval 3 and the central rod. Once the loss of integrity of interval 3 occurred, the extraction rate in interval 3, and the injection in interval 1 were stopped leading to a progressive decrease of the pressure in that interval, down to 19.5 bar. The pressure in interval 1 was set to this value on August 19th until September 18th when it was increased up to 25 bar. The leakage in interval 3 no longer allows the quantification of the extraction rate within this interval and the subsequent well effective permeability of the cemented annulus. Nevertheless strong sealing between interval 1 and 3 allows to continue the constant head injection of CO$_2$-rich pore-water within interval 1 at 25 bar during 6 more months (up to March 18th 2015). A total mass of 498 g of CO$_2$ has been injected within interval 1 during the entire *stage B*.

3.4. On-line fluid monitoring and fluid sampling for analyses at laboratory

At the end of the *stage A*, several sensors have been added to the extraction line (between the flow controller and the vial) to assess continuously the interval 3 fluid property changes during *stage B*:

- Upstream of the flow controller, pH and Eh probes (digital output; Hamilton Polilyte Plus Arc 120 for the pH sensor and Hamilton Polilyte Plus ORP Arc 120 for the Eh sensor). These sensors can
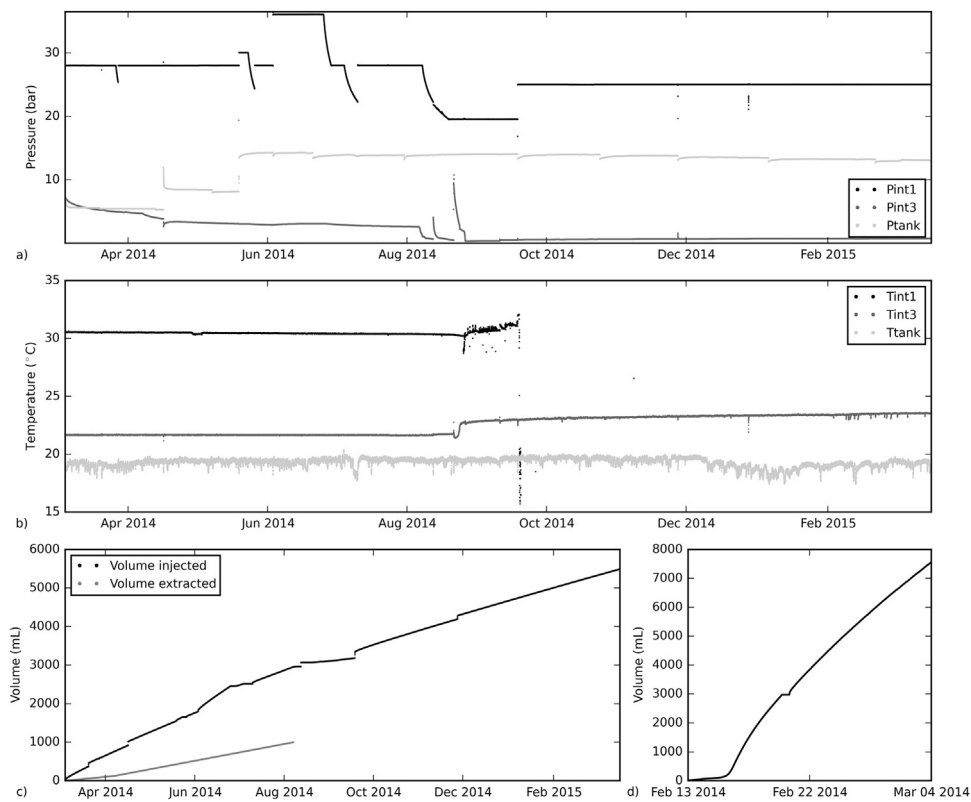
---

[1] Pee Dee Belemnite.

Fig. 2. Raw data recorded during *stage B*—a) pressure of intervals 1 and 3, and of the pressure tank in which CO_2 is dissolved/b) temperature of interval 1 and 3, and of the pressure tank (the temperature sensor of interval 1 stopped functioning in September 2014)/c) injected volume of carbonated brine in interval 1 and extracted volume in interval 3 since the beginning of stage B/d) volume of CO_2 injected in gas phase in interval 1 at the beginning of period 4.

be used for temperatures ranging between 0 and 140 °C and for a pressure of up to 16 bar;

- Downstream to the flow controller, one bromide probe (analogue output 0–2 V, with a control unit).

Three by-passes with peek/Plexiglas flowthrough cells have been installed for pH, Eh and bromide probes.

In parallel, fluids have been regularly sampled in intervals 1 and 3 for their chemical analyses at laboratory. Some fluid samples were collected by opening the interval flow line and after purging the flow line of its volume (*direct sampling*). Fluid from interval 3 was mostly sampled after the flowmeter where the vial is progressively filled by the solution extracted from the interval (*continuous sampling*).

Chemical analyses included major cations (K, Na, Ca, Mg, Sr) and anions (Cl, Br, SO₄), dissolved organic carbon (DOC), total inorganic carbon (DIC) and δ¹³C of DOC and DIC when possible. Analytical procedures are given in Appendix B of Supplementary material.

3.5. Stopping of the system and short hydraulic tests with gas

On March 18th and 19th 2015, the system has been stopped prior to the overcoring operations. The CO_2-rich water filling interval 1 was removed to avoid any exsolution. The pressure was maintained with N_2 at 25 bar through line P1 (upper line of interval 1), while the water was extracted in a pressure vessel through line Q1 (lower line).

After this step, most of the water had been removed from the intervals but the temperature and pressure conditions were not significantly changed. Given these similar conditions, a hydraulic test has been done to compare the hydraulic properties of the well under 100 % water-saturated conditions vs. under gas presence.

Since larger flow paths were suspected at the top of the cemented annulus after the observations made during *stage A*, resin mixed with fluorescein (used as a fluorescent tracer) has been injected in interval 3 with the aim of detecting the resin flow paths and thus of imaging these interfaces at least at the top of the cemented well-system. The injection was performed at approximately 2 bar.

3.6. Overcoring operations and complementary analyses on fluid and solids

The initial plan was to overcore the well-system with a 350 mm-diameter tool in order to retrieve the well system and the surrounding claystone. The operations started on March 30th 2015, from the initial depth of the pilot borehole (4.6 m) to the beginning of the cemented annulus (8.15 m). However, it appeared that the clayrock was milled during those operations, while the cement sheath remained intact. The overcoring operations were stopped and an additional borehole (borehole BCS-5A) was drilled from depth 8.15 m to depth 12.18 m on April 8th 2015 with the triple core technique (inside diameter 71 mm/outside diameter 86 mm) to sample clayrock close to the clay/cement interface (see Fig. 1c). The distance between the clay sampling and the interface is estimated to be approximately 15 mm. The operations have been resumed to complete the overcoring and the well-system has been lifted out of the borehole on July 1st 2015 (core BCS-5OC).

Claystone samples were characterised at six different depths of BCS-5A: 8.45–8.59, 9.46–9.58, 10.02–10.10, 10.15–10.18 (only for CO_2 partial pressure measurement), 10.65–10.74 and 12.08–12.13 m. Cation exchange capacity, aqueous leaching, carbon and oxygen isotopes of calcite, and CO_2 partial pressure measurements were performed on these samples. The three core
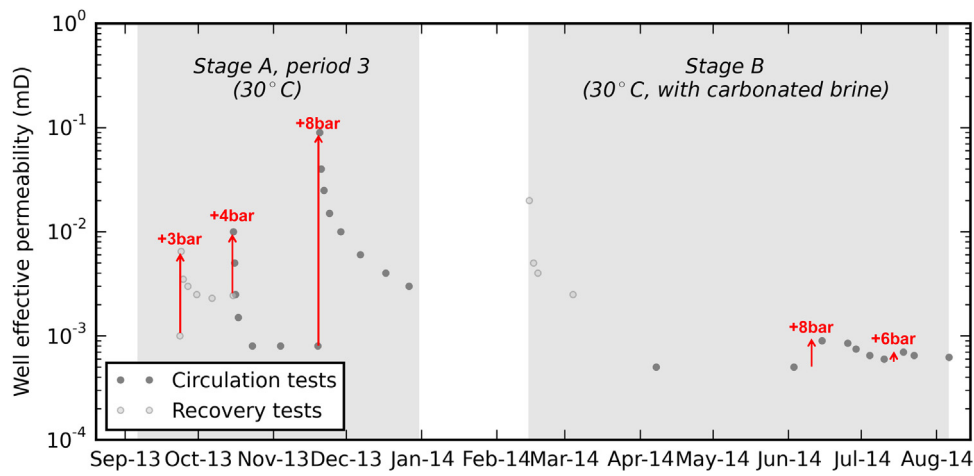
Fig. 3. Estimated effective well permeability over time during stage B; stage A, period 3 (from Manceau et al., (2015)) is also shown and the pressure steps set in interval 1 are also indicated.

samples near interval 1 of CO_2 injection: 10.02–10.10, 10.15–10.18 and 10.65–10.74 m were cut into two half vertical parts corresponding to a half near the interval 1 and a half further from the interval 1. The core BCS-5OC was sampled at five different depths: 8.32, 8.84, 9.54, 9.79 and 10.12 m. Microscopic observations as well as carbon and analyses of oxygen isotopes of calcite were carried out. The analytical protocols followed for the analyses are provided in Appendix B of Supplementary material.

4. Results

4.1. Hydraulic observations during stage B

4.1.1. Well effective permeability inversion

For *stage B*, the effective well permeability has been determined based on the same inverse modelling procedure than that used for *stage A* and presented in Manceau et al. (2015). A 2D-radial numerical model has been developed using TOUGH2 code (Pruess et al., 1999). The model radial extension is 100 m, with 3901 cells. The cement sheath permeability was used to represent the effective well permeability; the other influential input parameters were the caprock permeability, the intervals' compressibility, and the boundary conditions in terms of formation pore pressure. Similar values of caprock equivalent permeability to those used at the end of *stage A* were re-used for the beginning of *stage B* (i.e. 1.5×10^{-4} mD for the caprock in connection with interval 3, and $3. \times 10^{-5}$ mD for the caprock in connection with interval 1). The dynamic model results obtained at the end of *stage A* were logically considered as initial conditions for *stage B*. A major uncertainty concerned the compressibility of interval 1 and 3, which could have been influenced by the presence of gas that would not have dissolved properly. Interval 1 compressibility has been computed during the three pressure steps performed in that interval: 1.29×10^{-9}, 1.18×10^{-9} and 1.28×10^{-9} Pa^{-1} have been measured, showing similar values to values measured during *stage A* (1.3×10^{-9} Pa^{-1} had been considered) and therefore confirming the complete dissolution of the injected gas. Since no water has been directly injected in interval 3 during *stage B*, the compressibility of interval 3 could not have been measured with precision. This parameter has been considered equal to its *stage A* value (2×10^{-8} Pa^{-1}), after the verification that no gas exsolution occurred during fluid migration towards the interval 3.

This exsolution potential has been evaluated with a multi-step modelling procedure assuming that fluid flow prevalently occurs in the experimental apparatus through a channelized path at the cement-caprock interface (annulus). The calculations have been done with PHREEQC v.3. (Parkhurst and Appelo, 2013), a code able to simulate real gas behaviour by means of the Peng-Robinson equation of state. The goal of these calculations is to evaluate if, and, under which conditions, the water injected into the experimental apparatus (via interval 1) can release (by depressurization) a free gas phase, and if this free gas phase can accumulate in the interval 3. Fixing the chemical composition of the aqueous solutions present in the intervals 1 and 3, the numerical results sensitively depend on (i) the injection pressure of gases in the refilling tank, (ii) the confining pressure of interval 1, (iii) the pressure/temperature path of the fluids propagating along the annulus, and (iv) the amount of fluids from interval 1 effectively transferred through the annulus into interval 3. The minimum amount of interval 1 water required to have free gas accumulation in the interval 3 has been estimated to about 1.5 L, significantly above the volume estimated via hydraulic modelling (0.220 L over 6 months). This order-of-magnitude estimation corresponds to a conservative scenario that considers that all the gas possibly released from interval 1 waters, during a linear P,T decreasing path from interval 1 (30.5 °C, 28–36 bar) to interval 3 (21.7 °C, 3.9 bar) average initial conditions, has been effectively transferred into interval 3, without any loss into the adjacent caprock formation. Any possible dilution with caprock pore water, and/or gas loss into the caprock would increase (even significantly) this threshold value.

The results of the hydraulic modelling for *stage B* are provided in the appendices (Fig. A1 of Supplementary material); only the period before the loss of integrity in interval 3 could have been modelled. Note that the caprock permeability at the interval 1 level has been considered constant throughout the experiment. The good matching between the observations and the modelling results in terms of injected water volume validates this assumption. The equivalent caprock permeability at the interval 3 level has been considered constant at the beginning of stage B, but around day 50, the results of the initial model started to deviate from the observations; a slight increase has been set to mimic the observed behaviour of interval 3 pressure (2×10^{-4} mD instead of 1.5×10^{-4} mD). One potential explanation for that necessary modification is likely to be due to the change of flow direction (above 5–6 bar in interval 3, the pore water flows from interval 3 towards the caprock), which cannot be properly modelled with the initial parameters.

The evolution of effective well permeability during *stage B* is displayed in Fig. 3 together with that of *stage A*/period 3, corresponding to similar temperature conditions in the well (only the fluid composition has been changed). We see that during *stage B*,
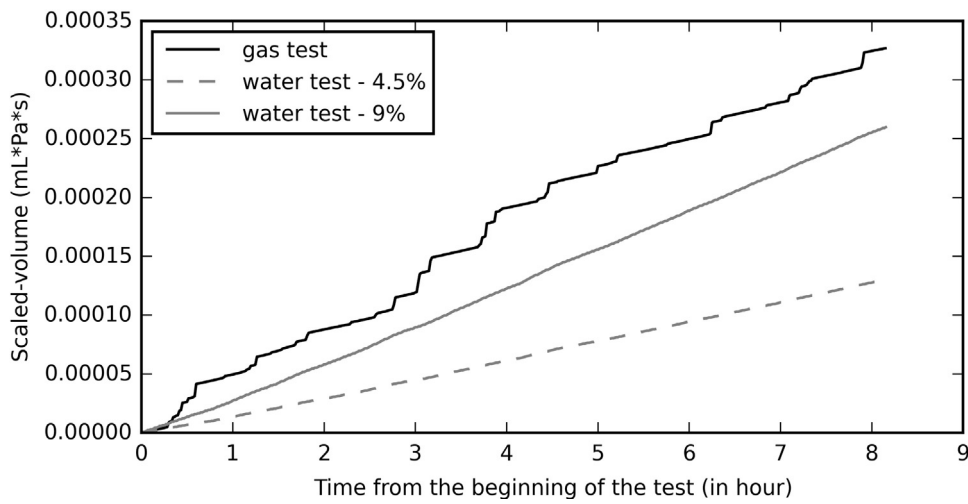
Fig. 4. Scaled-volume flowing along the well-system with pore-water and gas at similar conditions (2 scenarios of pore-water volume are shown corresponding to two fractions of the total pore-water volume injected in interval 1, respectively 4.5 and 9 %).

the effective permeability values remain lower than during *stage A*, period 3 even though the lowest values are in the same range for the two time periods (ca. 1×10^{-3} mD). The major difference is the response to the pressure steps imposed in interval 1 during the circulation steady state. Three pressure increases in interval 1 had been completed during *stage A*, period 3 similarly to during *stage B*. These changes had led to significant increase in the effective well permeability, while these increases seems much lower during stage B (see Fig. 3, note that the first pressure increase of *stage B* in May 2015 does not lead to any observable change and is not represented on the figure).

4.1.2. Hydraulic tests with gas

Just before stopping the system, the well-system has been kept at the same pressure and temperature conditions (25 bar, 30 °C), but with the replacement of the water filling the intervals by gas (N_2). Given the fact that the capillary pressure magnitude in Opalinus Clay is likely to be significant and therefore to restrain gas flow towards the formation (see for instance Fig. 4 of Croisé et al. (2006)), one can consider in a first approach that most of injected gas flows along the well-system. This volume injected after the replacement, has been compared with the volume estimated to flow along the well-system just before the replacement. Since the injected pore-water was flowing both towards the caprock formation and through the well-system, the fraction of the injected carbonated water flowing through the well-system had to be estimated. During the modelled period of *stage B*, this fraction had an average value of 4.5% and was always lower to 9%. Since our purpose was to compare permeability-like quantities, the volumes have been scaled by the inverse of the fluid viscosity. These scaled-volumes are plotted in Fig. 4 for a fraction of injected brine flowing along the well system of 4.5% and of 9%. For both cases, the scaled-volume of injected water appears to be lower than that measured during gas tests but of the same order of magnitude. Despite the uncertainties linked with this analysis (some gas might have entered in the caprock formation, the pore-water fraction flowing along the well-system might be different from the estimations), it would indicate that the well effective permeability measured all along this study in fully water-saturated conditions is not significantly different from the effective permeability that would be used to quantify gas advancement front migration.

4.2. Geochemical observations during stage B

4.2.1. Evolution of pore-water composition in interval 3

The compositions of the solutions sampled in Interval 3 are reported in the Appendix C of Supplementary material (Table C1). The bromide tracer content (Fig. 5a) is of particular interest since its evolution is related to an arrival of water flowing from the injection interval. The bromide concentration of interval 3 was stable before CO_2 injection and during the 2 first months after CO_2 injection. Then, its concentration starts to increase up to 2–2.5 times the Br initial concentration, about 3 months after CO_2 injection starts. The Br concentration that was reached during the arrival of the tracer still remains in the range of Br concentration in the Opalinus clay pore water, but the evolution of the Br/Cl ratio confirms that the Br increase is due to the arrival of a Br rich water with a different Br/Cl ratio than the Opalinus clay pore water. The Br evolution in interval 3 is then most likely the indication of an arrival of Br-marked water from interval 1.

In contrast to the Br non-reactive tracer evolution, the isotopically marked injected CO_2 is not observed in interval 3 (Fig. 5b).
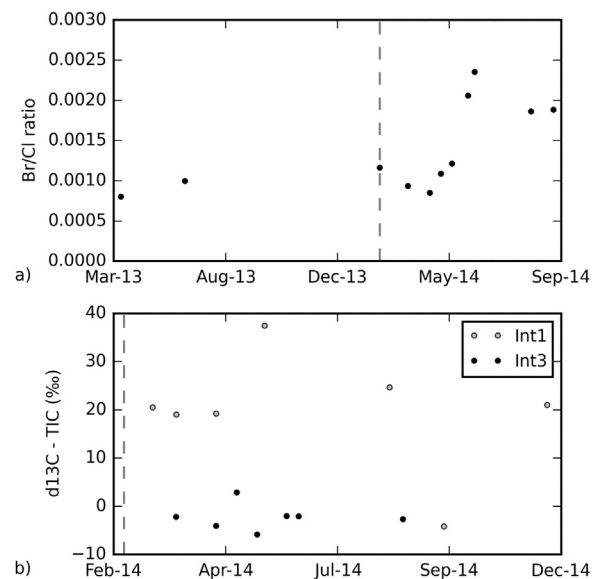

Fig. 5. a) Evolution of Br/Cl ratio in interval 3; b) Evolution of interval 1 and 3 water isotopic signature. The dashed vertical line indicates the beginning of stage B.

Indeed, the δ^{13}C-TIC signature remains constant over the experiment duration, in the range of its initial signature, while the δ^{13}C-TIC signature in interval 1 shows higher values, notably differentiated from initial pore water. It suggests that the injected CO_2 has reacted along its flow path between interval 1 and interval 3 (potentially by the precipitation of calcite).

In parallel to this change of Br concentration, some elements (Ca, Na, Mg, Sr, Si, SO_4, Cl) present some small variations in their concentration, displaying either an increase or a decrease. The variations are relatively moderated but they are observed simultaneously and correspond to the samples in which a Br arrival has been evidenced.

The pH is stable in interval 3 (Appendix C of Supplementary material, Fig. C1) during the period where CO_2 was injected in interval 1. The pH measured by the in-line sensor is considered as more reliable since it is measured at the interval pressure and, then, does not suffer CO_2 outgassing during the sampling and the analysis. The redox potential was measured in-line at the outlet of interval 3 (Appendix C of Supplementary material, Figure C 1) and was also calculated from the measured Fe^{2+} and total Fe concentration (Appendix C of Supplementary material, Table C 1). The in-line measured Eh first shows a decrease and then stabilizes at a value of about -560 mV. The decrease is due to the arrival of water from interval 3, which replaces the water used for the saturation of the Eh sensor by-pass lines. The stabilized negative Eh values, corresponding to reductive conditions, are then considered as representative of the redox conditions in the interval. The Eh sensor was calibrated at several times, confirming the measured Eh values. Measured Eh values are lower than the Eh obtained in other experiments at Mont Terri (usually between -250 and -400 mV (Wersin et al., 2011)). The positive calculated pe values obtained from the water samplings are not consistent with the in-line measurements and, then, indicate that the water were oxidised once sampled from the interval.

4.2.2. Insights from pore water composition evolution, and expected mineralogical evolution of the well system

Based on P,T conditions of the experimental apparatus, and constraints from hydraulic modelling, a set of reactive transport calculations has been performed with TOUGHREACT v.2 (Xu et al., 2012) to evaluate the geochemical processes induced by the propagation of carbonated waters through the annulus. The model has a pseudo-2D geometry (Fig. 6) and considers a simplification of the different domains through a multi-porosity approach, including properties reasonably representative of the average properties of the compartments of interest (intervals 1 and 3, annulus, caprock). In particular, the annulus has been modelled as a single domain with a vertical permeability of 1.5×10^{-18} m^2. The different domains are aligned along the vertical extent of the well and mass exchange at lateral boundaries (such as at the annulus-caprock interface) is allowed. The initial geochemical conditions are given in the appendices (Table A1). The model considers the annulus to have the initial geochemical properties of cement, which is by far more reactive than the adjacent caprock. Volumes, interface areas, internodal distances, effective porosity, permeability of the different compartments are key parameters that sensitively affect the numerical outputs, calibrated by trial-and-error to obtain reasonable fitting with experimental data on tracer concentration. The water flow between the intervals, the caprock and the annulus obtained by inversion of the pressure evolution using the hydraulic model were considered as input parameters of the reactive model. The matching between numerical and experimental data is intrinsically non-linear, and given the quite large number of parameters involved, it is not possible to identify a unique "best fitting solution". Fig. A2 of Supplementary material shows an example of good fitting conditions, achieved by following this
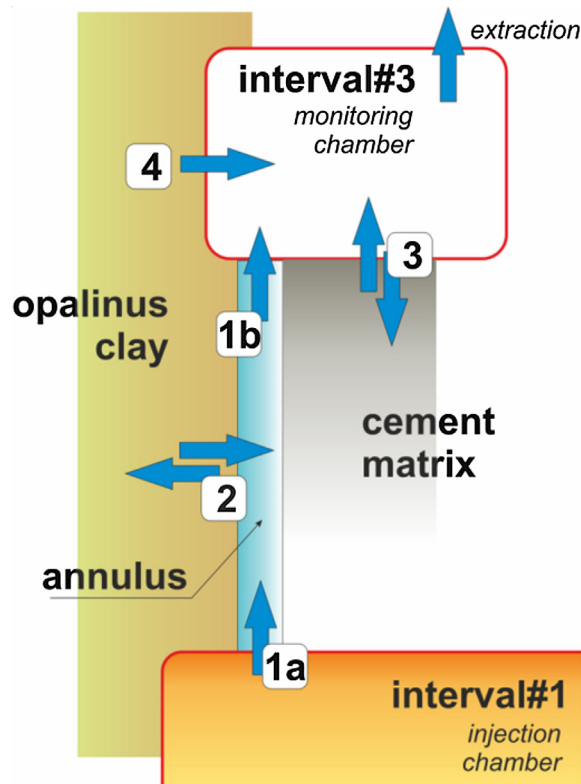

Fig. 6. Conceptual model used for reactive transport simulations. Blue arrows represent mass exchange between different compartments considered in the model: 1a = from interval 1 (injection chamber) to annulus; 1b = from annulus to interval 3 (monitoring chamber); 2 = caprock-annulus; 3 = from cement sheath to interval 3; 4 = from near-apparatus environment to interval 3. (For interpretation of the references to colour in this figure legend, the reader is referred to the web version of this article.)

iterative approach. Mass balance in interval 3 is controlled by the predominant contribution of fluids propagating from the interval 1 (injection chamber), and flowing through both the annulus and the portion of the caprock adjacent to cement interface. Under these conditions, the propagation of pH-acid, CO_2-rich fluids coming from interval 1 causes a significant decrease of the pH in the aqueous solution permeating the annulus. In this compartment, the pH rapidly stabilizes between 8.2–8.3, well below the initial value of ~12.4. The reactive flow through the annulus also causes an increase of the total concentration of most of the aqueous constituents (Si, S, Mg, Sr, Br). Only Ca tends to decrease because of mineral dissolution/precipitation processes. Over the 6 months of simulation, the main mineralogical transformations predicted by the code (Fig. 7) are a minor dissolution of most of the primary solid constituents of the cement (portlandite, CSH(1.6), ettringite, hydrogarnets: C_3FH_6 and C_3AH_6), and the precipitation of calcite, hydrotalcite, and traces of amorphous silica. Overall, the mineralogical facies of the cement sheath is negligibly affected by water-rock interactions, and a minor decrease in porosity is predicted ($-4\permil$) over the 6-month period of hydraulic test, which can be converted to a net volume of 2.2×10^{-7} m^3. It is noteworthy that the reactive model implemented here (where fluids of mixed composition from caprock, cement and interval 1 interact with the primary mineralogy of the cementitious annulus) underestimates exchanges between the annulus and the lateral domains (caprock, and possibly cement matrix). Thus, the lateral inflow of caprock fluids is underestimated, which also means that an additional 'sealing process' could be neglected if additional phases form by reaction of the caprock water and CO_2.
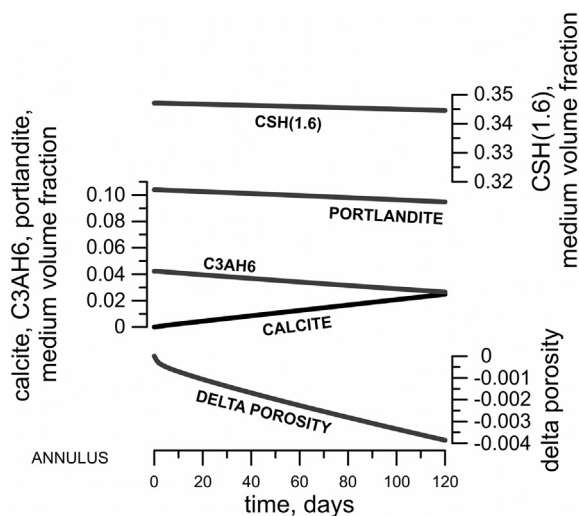
Fig. 7. Porosity and medium volume fraction variations for selected solid constituents (CSH(1.6), portlandite, C3AH6, calcite) in the annulus compartment.

Considering the average effective well permeability inferred from the hydraulic tests and used in the reactive transport simulations (1.5×10^{-18} m^2), the equivalent thickness of the annulus computed by the cubic law would be 7.7×10^{-7} m^2; with that geometry, the estimated net volume change would correspond to a vertical extent of complete sealing of 46 cm.

4.3. Observations after overcoring

4.3.1. Observations during the overcoring stage and inspection of the retrieved well-system

4.3.1.1. Good quality cementing process. The cement sheath appears to be an impression of the initial borehole wall drilled in the clay-rock, indicating a good cohesion between cement and clayrock even in fractures/shear planes (see Fig. 8-1). This would indicate that 1) the cementing was mostly of very good quality and 2) the cement bulk was not crushed during the overcoring operations, i.e. the external part of the well-system recovered after the overcoring operations would be close to the cement/clay interface.

4.3.1.2. Presence of a micro-annulus at the cement/clay interface. As indicated in Section 3.6, clay was milled during the overcoring while the cement remained quasi-intact: this clay crushing could be linked with the interface clay/cement weakness, (and by the difference of mechanical properties between clay and cement). To check the hypothesis of a micro-annulus existence at that interface, a video was made during the overcoring operations, when the overcore drilling was at a depth of 8.15 m (i.e. in the upper part of the cemented well system). In Fig. 8-2, the interface clay/cement is visible and micro-annulus can be observed. However, it is difficult to know if this space existed anterior to the overcoring operations or if it has been created by this stage.

As described in Section 3.5, resin and fluorescein have been injected in interval 3 before stopping the system with the aim of localizing these flow paths. The external upper part of the cemented well system corresponding to the cement/clay interface located close to interval 3 has consequently been observed under UV illumination after its retrieval: a green coloration has been noticed (see Fig. 8-3), indicating the presence of fluorescein and therefore confirming the existence of a flowing path at this level.

The observation of flow pathways at the clay/cement interface appears to be in line with the conclusions of *stage A* obtained by hydraulic and geochemical modelling.

4.3.1.3. Good bonding at the cement/steel interfaces. The well-system lifted out (see Section 3.6) was almost intact, only a small crack has been noticed in the upper section of the system at the location of the cable used for the lifting. Therefore, the bonding between the cement sheath and the steel casing appears to be of very good quality: despite the strong mechanical effort put on the system during the overcoring process, no lack of bonding has been observed. The cross section of the well-system sawed at a depth of 10.05 m is shown on Fig. 8-4: all the cemented steel interfaces are of good quality and no visible micro-annulus has been noticed. The exposition to UV light of the cement/steel interface at the same depth than in Section 4.3.1.1, did not show any presence of fluorescein, confirming the absence of significant flowing path.

4.3.1.4. Signs of cement carbonation along the cement/clay interface. The entire 2.3 m long section show signs of carbonation (grey-ish colouring) on the external side of the cement sheath (initially in contact with the clay): this was confirmed with HCl testing. However, the appearance is slightly different for the 40 cm section located at the bottom of the cemented well system where a yellow/orange colouring can be seen.

4.3.1.5. Signs of cement carbonation along the cement/steel interface. After removing some of the cement sheath from the casing, the interface cement/steel was observed. A white precipitate has been observed at that interface. No clear difference has been observed between different samples taken at different depths, which indicate a relatively homogeneous precipitation. HCl testing confirmed the presence of carbonates.

As indicated above, the cement sheath integrity was very good, and no sign of significant cracks through this sheath have been found. However, one small fracture across the cement sheath has been observed. Interestingly, carbonation within the fracture can be observed, which would indicate a self-sealing of the fracture (Fig. 8-5).

4.3.1.6. Signs of casing corrosion. At the very top the well-system (depth 7.82–7.95 m), a zone with no cement has been noticed. The casing was damaged and corroded at that level, and a breach has been observed within the steel. It is unlikely that this hole has been created during the overcoring operations given the very good state of the well-system that has been lifted out, and its appearance seems to indicate that this hole has been created by corrosion. Interestingly, the observation of the casing steel on a larger zone shows that the corrosion was very localized to the "no-cemented" zone and that the steel casing was very well protected by the cement sheath even very close to this damaged zone (see Fig. 8-6).

4.3.2. Characterization of the claystone core (BCS-5A)

4.3.2.1. Carbon and oxygen isotopes in calcite. Calcite extraction and carbon isotopes of calcite were performed to trace potential modifications of the carbonate fraction due to CO_2 injection in the claystone. The δ^{13}C and δ^{18}O of the calcite in the claystones range between 0.3 and 0.4‰ (PDB), and between 24.4 and 25.0‰ (PDB) respectively. These isotopic values are homogeneous whatever the position of the claystones relatively to the experiment system, and are almost similar to the carbon and oxygen isotopic compositions of calcite in unperturbed Opalinus claystones.

4.3.2.2. Cation exchange capacity (CEC) and aqueous leaching on claystone. Cation exchange capacities (CEC) were measured in claystones in order to test potential perturbations of the sorption capacity and of the sorbed-cation distribution of clay minerals (Table C2 of Supplementary material). The CEC and the concentrations of exchanged cations (given in meq/100 g of rock) measured in claystones from this experiment differ slightly from reference
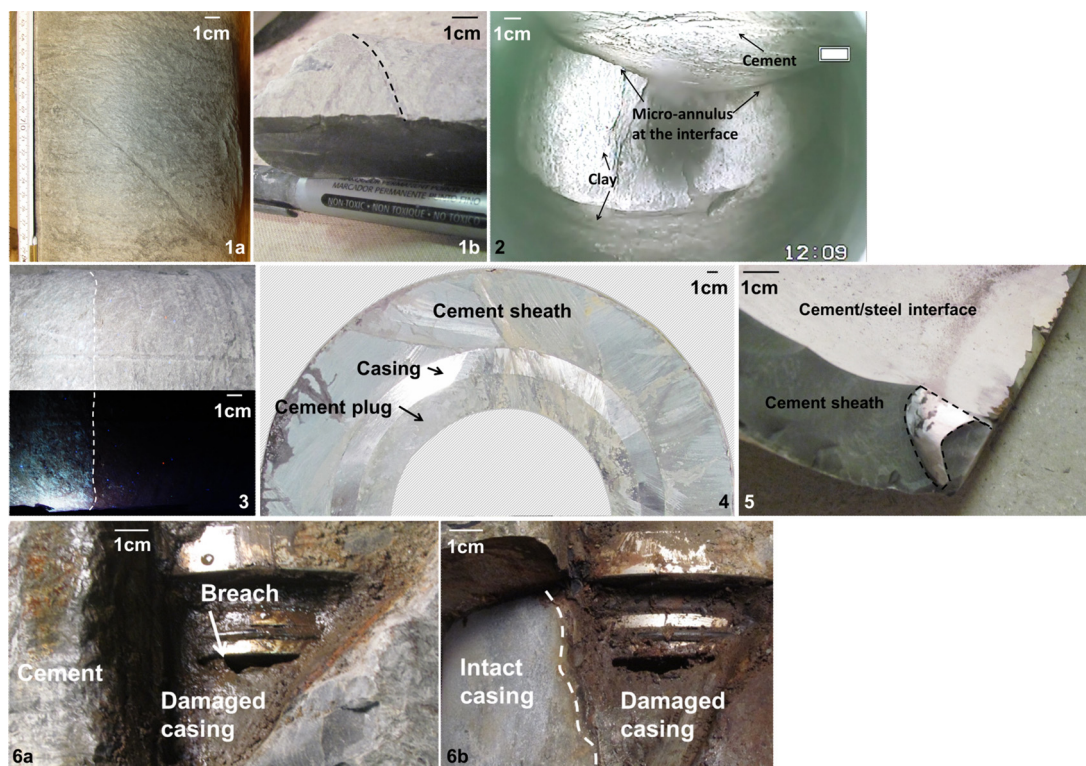
Fig. 8. Inspection of the retrieved well system: 1—a) shear planes "footprints" on the external part of the well system; b) No impact of the shear planes within the sheath (the shear plan footprint is highlighted with dotted line) 2—Borehole inspection made after the overcoring the system until depth 8.15 m 3—Photograph of the same piece of the cemented well-system under normal light (top) and ultraviolet light (bottom). The picture corresponds to the cement/clay interface at depth 8.16–8.36 m (the advancement front until which the resin seems to have hardened is indicated with a dotted line) 4—Half cross section of the cemented well-system sawed at depth 10.05 m) 5—small crack across the cement sheath sampled at depth 9.92 m (dotted zone) 6—Signs of casing corrosion. a) Breach in the casing at a non-cemented zone level b) same picture after cement removal: intact casing outside of the damaged zone.

values by a lower Mg concentration and a higher K concentration. These variations are low and could be due to the natural heterogeneities of the clay formation. The Sr concentrations measured in the sample BC5-12.08 m are abnormally high, and combined with high sulfate concentrations in the leachates strongly suggest the presence of celestite (strontium sulfate) in the sample.

Aqueous leaching was performed in claystone to access to the anion concentrations (Cl, SO_4, Br) in pore water, and to detect Br tracer. Br measurements were too low to detect any diffusion into the claystone. The Cl concentrations measured in samples from this experiment are almost comparable with or slightly higher than reference values of Opalinus claystone at the level of the casing. They slightly increase in claystones samples near the interval 1 (CO_2 injection). Values measured in the same core samples at the level of the interval 1 but nearer and further from the interval also exhibit a decrease of the Cl concentration with the distance. The sulfate concentrations measured in samples from this experiment are almost comparable with reference values of Opalinus claystone, except the sample BCS5-12.08 m.

According to these analyses on claystone samples, the CO_2 injection did not induced noticeable degradation of the caprock formation.

4.3.2.3. CO_2 partial pressure measurements. Monitoring CO_2 outgassing of core claystone samples and analysing $\delta^{13}C$ of CO_2 was a way to detect any diffusion of the CO_2 tracer into the claystone. CO_2 partial pressures (pCO_2) and $\delta^{13}C$ of CO_2 were compared with reference values. The pCO_2 measured in unperturbed Opalinus Clay ranges between 3.6 and 8.9 mbar (minimum time of equilibrium of 3 months), and corresponding $\delta^{13}C$ of CO_2 is about −11.5‰

(Gaucher et al., 2010; Lerouge et al., 2015). In this experiment, the equilibrium regarding pCO_2 between minerals and pore water is not expected to be achieved.

The analyses were performed a short time after conditioning (for analysing the most available CO_2) and a longer time after conditioning. The raw data are provided in the Appendix C of Supplementary material (Table C 3). The CO_2 outgassing of the nine glass containers were compared to outgassing of Opalinus claystone references. At 27 days, four samples at depth 8.55 m, 10.15 m (near), 10.65 m (near) and 12.08 m provided evidence of abnormal high CO_2 outgassing. At 161 days, all the pCO_2 values are higher than references values obtained for unperturbed claystones. The CO_2 extracted at 2 days showed abnormal high $\delta^{13}C$ in claystones near the interval 1, and specifically at the bottom of this interval 1, and at the level of the casing − depth 8.45–8.55 m. After 69 days and a first gas extraction, the $\delta^{13}C$ remains abnormally high in claystones near the bottom of interval 1. Two populations of samples are distinguished:

1) A first population of samples, the least perturbed, exhibit an almost similar range of pCO_2 around 14–16 mbar and the lowest $\delta^{13}C$ of CO_2 between −12 and −7‰; values of 14–16 mbar remain higher than reference values measured in previous works (Lerouge et al., 2015). Recent experimental work provided evidence of an increase of pCO_2 with the relative humidity and the saturation state of the sample (Lassin et al., 2016). Reference pCO_2 were measured on samples from a drillhole drilled with Ar flux and without any resaturation, with a maximum relative humidity measured at ~95%. In the present system, the initial borehole was entirely resaturated with synthetic Pearson pore water.
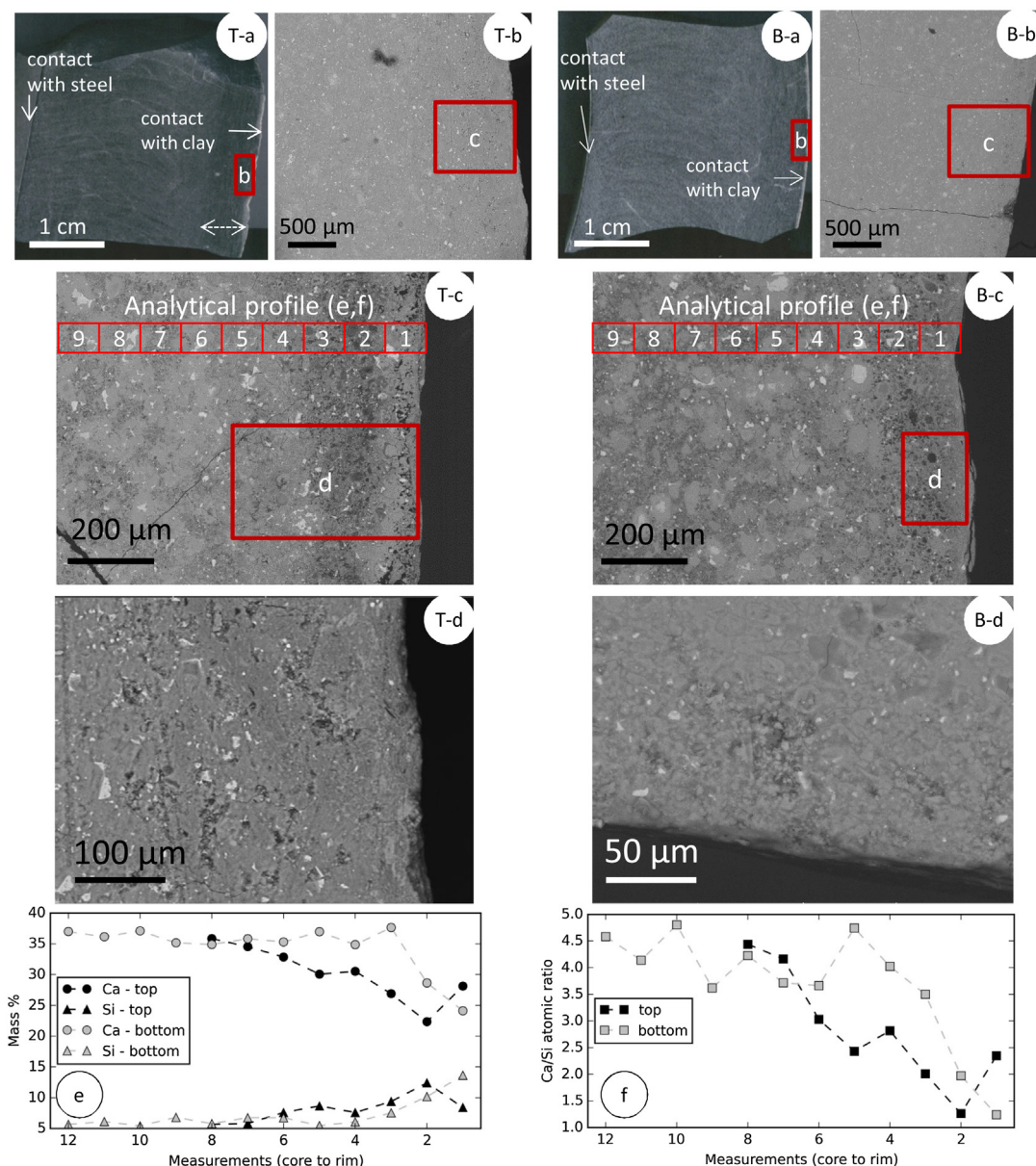
Fig. 9. Aspect at different scales of the cemented annulus at the top of the well-system (index T) and at the bottom (index B): (a) Polished cross-section showing the different texture of the cement; (b, c and d) Focus on the cement on the external side in contact with clay. Chemical composition of the cemented annulus close to the contact with clay: (e) Ca and Si contents (given in weight percent), measured on surfaces along a radial profile at the top and bottom of the well-system (cf. figures c); (f) corresponding bulk Ca/Si atomic ratio calculated along a radial profile at the top and bottom of the well-system.

2) A second population of samples exhibit significantly higher pCO_2. At the level of the interval 1, these high pCO_2 are associated to abnormal high $\delta^{13}C$ of CO_2, corresponding to the migration of the injected CO_2.

The sample BCS5_ 8.45–8.55 m has a first $\delta^{13}C_{CO2}$ value of +24.6‰ and a second one of −6.2‰; these data combined with O_2 and N_2 concentrations indicate that the claystone at this depth was highly perturbed. The BCS5_12.08–12.12 m (below the interval 1) showing a leak of the glass container does not have abnormal $\delta^{13}C_{CO2}$ value (−7‰).

To conclude, the impact of the CO_2 injection is evidenced at the surrounding of the interval 1, interval in which CO_2-rich water was directly injected; elsewhere in the upper part of the system there is no evidence of impacts of the injected CO_2.

4.3.3. Characterisation of the overcore cement (BCS5-OC)

4.3.3.1. Microscopic observations. Microscopic observations of polished cross-sections of the cement casing at 7.8–8.8 m (top) and at 10.12 m (bottom) provided evidence of almost homogeneous texture and chemistry of the cement except on the cement interfaces with clay and with steel (Fig. 9). The carbonation detected by microscopic observations and HCl tests is confirmed by SEM. The cement in contact with steel is just characterised by the formation of a 20 μm-thick calcite coating. The cement in contact with claystone exhibits a visible external 5 mm-thick zone with a different texture probably due to creep during hardening and different rate of hydration of the cement (Fig. 9a). The cement on this side shows a surface perturbed by the drilling which consists of a mixing of crushed clay and cement paste. In addition, the first 200–300 μm thick zone of cement close of the cement/claystone interface is more porous and
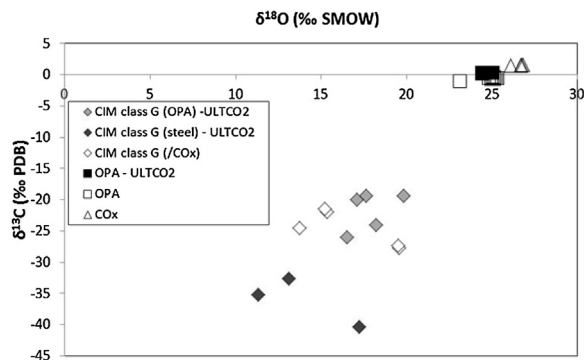
Fig. 10. $\delta^{13}C$–$\delta^{18}O$ diagram showing data from calcite extracted in clay formation and in cement at both interfaces (clay and steel). Data from the same type of class G cement in contact with Callovian-Oxfordian clay formation are given for comparison (Gaboreau et al., 2012). The data coming from this experiment are named "ULTCO2".

presents a Ca/Si ratio lower than in the rest of the cement (Fig. 9c–f). This data is consistent with previous studies on cement class G and classical Portland materials in contact with clay (Gaboreau et al., 2012).

It has to be noted that this perturbation appears, on Fig. 9, less obvious at the bottom than at the top of the well. However, the microscopic observations have shown, at the top of the well, some low-perturbed zone as well, indicating non homogeneous processes. No clear observation of generalized differences between the top and the bottom of the well could have been made.

4.3.3.2. Carbon and oxygen isotopes in calcite

In order to quantify and to determine the origin of calcite in cement on both interfaces (external interface in contact with Opalinus Clay and internal interface in contact with casing), the $\delta^{13}C$ and $\delta^{18}O$ of calcite were measured after performing a local attack of the cement with phosphoric acid (Table C4 of Supplementary material).

The $\delta^{13}C$ and $\delta^{18}O$ of calcite in cement in contact with claystone is significantly different from those of calcite in cement in contact with steel (Fig. 10). The ^{13}C enrichment in cement in contact with clay could be due to interactions with CO_2 from the clay formation, or to interactions with injected CO_2 ($\delta^{13}C \sim +20‰$). Comparison of these data with those obtained in similar class G cement in contact with Callovian-Oxfordian clay formation (Gaboreau et al., 2012) provides evidence of similar ranges of values. Consequently (C, O) isotopic data on cement do not support any formation of calcite linked to a migration of the injected CO_2, but rather show that the calcite was formed by precipitation of carbonates due to reaction with the claystone or with the synthetic solution. However it is noteworthy that calcite content in cement at interface with clay is lower at the bottom of the casing near the interval 1 of CO_2 injection (Table C 4). A lower calcite content could be explained by heterogeneities of clay/cement interactions or by a partial decarbonation of the cement due to the injected CO_2 migration.

5. Interpretation and discussion

The overcoring step has provided the opportunity to gain information usually not accessible or at high costs. It has confirmed the potential migration pathways that were expected by hydraulic and geochemical observations, and modelling performed during the operations. In our case, the migration along the well seems to have occurred mainly along the clay/cement interface. The increase of temperature at the bottom of the well has closed that interface progressively but the interpretation made after the first year of experiment (see Manceau et al., 2015) and the observations made

during and after the overcoring indicate that a micro-annulus was still present at the top of the well. It can be assumed that this micro-annulus was present at the very beginning of the experiment all along the well to explain the initial permeability of the well (20 mD), despite the care taken to perform the cementing. The explanation of that can be a shrinkage during the cement curing. Cement shrinkage can be due to several reasons as detailed e.g. in Dusseault et al. (2000): Water expulsion before hardening, less volume occupied by the cement after the hydration process, presence of dissolved gases, osmotic dewatering in strongly salted environment, high curing temperatures and early set are some of the given reasons. The three former reasons cannot be ruled out but the three latter do not correspond to the conditions of the experiment. In addition, the cement/clay interfaces appeared to be a fingerprint of the initial borehole wall and therefore the shrinkage, if it occurred, took place after hardening.

The continuous hydraulic tests have shown a diminution of the permeability increase potential with pressure increase after CO_2 was injected, compared with the previous period (*stage A*, period 3). This observation has been done in a specific context: In particular, the modelling of the hydraulic tests has shown that the effective permeability was very low during *stage B* and the advective fluid flow through the near-well environment was limited. In such conditions, the experiment indicates that even when forcing CO_2 rich water to enter the near-well environment, the contact with CO_2 leads to sealing of the initial flow pathways, and therefore an increase of the well integrity. Furthermore we did not notice any degradation of the well hydraulic properties, as it has been sometimes noticed, in advection dominated context (see Section 1). The question of how the well would have behaved with different pre-CO_2-contact hydraulic conditions is an open question. Nevertheless, the experiment provides interesting insight regarding the effect of CO_2 when relatively good integrity pre-exists before a well is in contact with a CO_2 plume.

The precipitation of carbonates along flow pathways is suggested to explain the decrease of the wellbore effective permeability and the apparent sealing of the clay/cement interface. However, an influence of the injected CO_2 in the carbonation could not have been measured in the cement sampled in the well-system. This could be explained by 1) the precipitation of calcite occurring in limited amounts regarding the balance between the CO_2 in solution, the limited volume of migrating fluids (given the low initial effective well permeability) and the clayrock and cement volumes in contact with the flowing water; or 2) the absence of precipitation on the analysed cement samples. The most probable cause could be that the carbonate minerals that have precipitated at the interface between Opalinus Clay and cement have been lost during the overcoring (we recall that the claystone surrounding the cemented casing has been crushed during the operations). The precipitation of carbonates along flow pathways can nevertheless be supported by the consumption of the injected CO_2 during its migration along the well. This has been confirmed by the comparison between the non-reactive tracer evolution (that has reached the interval 3 after its co-injection with CO_2) and the reactive tracer evolution (the isotopically marked CO_2 was not detected in the upper interval). Moreover, according to the reactive transport modelling results, the precipitation extent was limited but it could have induced the clogging of a small-size pathway on a non-negligible height.

The claystone samples analysed showed a very low circulation of CO_2-rich water through that rock, limited to the zones located very close to the high-pressure injection interval. Even in that zone, the detection of the injected CO_2 mainly during the first outgassing suggests that the CO_2 was in the claystone porosity and not incorporated in the solid phase. No evidence of migration through a potential BDZ have been found, nor degradation of the caprock close to the cement sheath before or after the well-system exposure to

carbonated pore water. These evidences support the good integrity of the clay-rich caprock formation, and its low influence on the equivalent hydraulic conductivity of the well.

The analyses and observations made on the cement bulk indicated that the cement material overall did not allow significant flow and that it accurately plays its barrier role, during all the stages of the experiment. This confirms that well integrity problems do not come from the cement material itself if good cementing practices are followed. A slight degradation has been observed at the cement/claystone interface, illustrated by an increase of the porosity and by the decrease of Ca/Si ratio in the cement along the well, to be linked to dissolution of portlandite and/or of Ca-rich CSH. No clear sign of additional effect of the injected CO_2 within this degradation could have been noticed.

The cement also appeared to provide a strong protection of the steel casing where cement was present, with no visible signs of alteration ca. 3 years after the well construction. However, the high corrosion noticed in one non-cemented zone highlights the importance of corrosion issues. It should be noted that the context of the experiment was very specific: Only the cement sheath was used as a protection against corrosion, and the steel casing section was connected to the experimental set-up (packers, tubes) made of other materials (notably stainless steel) in an electrolyte environment (salted water, according to the analyses the injected CO_2 is not likely to have reached that zone and thus to be involved in the corrosion), which could have favoured a galvanic corrosion type. The observed corrosion nevertheless shows the importance of corrosion preventive measures implementation, such as corrosion inhibitors, and cathodic protection (Talabani et al., 2000; Choi et al., 2013).

6. Summary and conclusion

A 1:1 scale experiment supported by multi-disciplinary analyses has allowed improvement of the understanding of the well integrity issue in the context of CO_2 geological storage. A well section has been constructed in the Mont Terri underground laboratory and the hydraulic and geochemical evolution of this section has been followed with the application of different stresses on the system (temperature, pressure and geochemical). The well system has been ultimately overcored for inspection. At the end of the experiment, a significant quantity of information of different types are accessible: Raw data or interpreted results from 2.5 year-long hydraulic tests, water composition at different time periods, observations and mineralogical analyses on overcored samples of the well system give the opportunity to explain the behaviour of the well-system during the experiment.

The first year of the experiment (stage A), when different pressure and temperature conditions were applied is extensively described in Manceau et al. (2015). This paper has been focused on the second year of the experiment (stage B) dedicated to the exposure of the system to CO_2-rich pore water and to the overcoring stage.

Two types of outcomes can be extracted from the results presented in that manuscript.

1) Key messages regarding the understanding of processes affecting the integrity of a well can be derived from the experimental results:

The relatively high initial well permeability (at the beginning of stage A) has been explained by a migration along the cement/clay interface, possibly due to cement shrinkage, while the cement matrix and the clay-rich caprock close to the well appeared to be a very good barrier to unwanted fluid migration. *This showed that the*

potential weakest points are interfaces between well elements rather than the well elements themselves, if appropriate materials are used.

The cement has correctly protected the steel casing from corrosion, except in one small area, where the cement sheath was absent and where the corrosion was important. *This showed that an appropriate cementing is compulsory to avoid issues regarding well integrity but also the importance of corrosion prevention measures implementation.*

The hydraulic conductivity of the well-system was significantly lowered during exposure to CO_2-rich pore water. In that context, the well integrity did not appear to have been compromised, but rather improved by the geochemical reactions. *This showed that, when good integrity pre-exists before a well is in contact with carbonated water, the exposure to dissolved CO_2 does not seem to lead to a degradation of the well hydraulic properties but rather to their improvement.*

2) This study confirms the ability of this type of experiment (1:1 scale in a controlled environment) to improve our knowledge on complex phenomena (thermal, mechanical, hydraulic and geochemical) occurring at a realistic scale, which is especially important for well integrity. Such experimental works may indeed allow an integration of a maximum of realistic processes, the monitoring of parameters usually only measurable in the field (e.g. effective well permeability) and the validation of the upscaling of laboratory results: *Similar experimental set-up could be used to study the impact of different types of controlled-defects in a well, or to test monitoring and remediation strategies to detect/correct any undesired fluid migrations along a well.*

As for *stage A*, it should be noted that the pressure, temperature and geochemical conditions range covered during *stage B* as well as the experiment duration were limited, and that the formation under study together with the well construction stages were specific to this experiment. Any generalization or extrapolation to longer time-scales of the experiments outcomes should therefore be considered with caution (Manceau et al. (2015)).

In addition, it should be noted that the present study is focused on well integrity understanding: For the assessment of potential migration impacts in a specific situation, the well integrity should be evaluated in parallel to driving forces in place (buoyancy, pressure gradient) and to the vulnerability of subsurface/surface stakes.

Appendix A to C. Supplementary data

Supplementary data associated with this article can be found, in the online version, at http://dx.doi.org/10.1016/j.ijggc.2016.09.012.

References

Abdoulghafour, H., Luquot, L., Gouze, P., 2013. Characterization of the mechanisms controlling the permeability changes of fractured cements flowed through by CO_2-rich brine. Environ. Sci. Technol. 47 (18), 10332–10338.

Bai, M., Sun, J., Song, K., Reinicke, K.M., Teodoriu, C., 2015. Evaluation of mechanical well integrity during CO_2 underground storage. Environ. Earth Sci. 73, 6815–6825.

Barlet-Guédard, V., Rimmelé, G., Porcherie, O., Quisel, N., Desroches, J., 2009. A solution against well cement degradation under geological storage environment. Int. J. Greenh. Gas Control 3, 206–216.

Bonett, A., Pafitis, D., 1996. Getting to the root of the gas migration. Oilfield Rev. 8 (1), 36–49.

Bossart, P., Thury, M., 2008. Mont Terri Rock Laboratory Project, Programme 1996 to 2007 and Results Rep. Swiss Geological Survey 3, Wabern, Switzerland.

R.A. Bruckdorfer, 1986. Carbon Dioxide Corrosion in Oil Well Cements, SPE Paper 15176, Billings, Montana, USA, May 19–21.

Carey, J.W., Wigand, M., Chipera, S.J., WoldeGabriel, G., Pawar, R., Lichtner, P.C., Wehner, S.C., Raines, M.A., Guthrie Jr., G.D., 2007. Analysis and performance of oil well cement with 30 years of CO_2 exposure from the SACROC Unit, West Texas, USA. Int. J. Greenh. Gas Control 1, 75–85.

Carey, J.W., Svec, R., Grigg, R., Zhang, J., Crow, W., 2010. Experimental investigation of wellbore integrity and CO_2-brine flow along the casing-cement microannulus. Int. J. Greenh. Gas Control 4, 272–282.

Carey, J.W., 2013. Geochemistry of wellbore integrity in CO_2 sequestration: Portland cement-steel-brine-CO_2 interactions. Rev. Mineral. Geochem. 77, 505–539.

Carroll, S., Carey, J.W., Dzombak, D., Huerta, N., Li, L, Richards, T., Um, W., Walsh, S., Zhang, L., 2016. Review: role of chemistry, mechanics, and transport on well integrity in CO_2 storage environments. Int. J. Greenh. Gas Control 49, 149–160.

Choi, Y.-S., Young, D., Nešić, S., Gray, L.G.S., 2013. Wellbore integrity and corrosion of carbon steel in CO_2 geologic storage environments: a literature review. Int. J. Greenh. Gas Control 16S, S70–S77.

Croisé, J., Mayer, G., Marschall, P., Matray, J.M., Tanaka, T., Vogel, P., 2006. Gas threshold pressure test performed at the Mont Terri Rock Laboratory (Switzerland): experimental data and data analysis. Oil Gas Sci. Technol. 61, 631–645.

Crow, W., Carey, J.W., Gasda, S., Brian Williams, D., Celia, M., 2010. Wellbore integrity analysis of a natural CO_2 producer. Int. J. Greenh. Gas Control 4, 186–197.

Duguid, A., Scherer, G.W., 2010. Degradation of oilwell cement due to exposure to carbonated brine. Int. J. Greenh. Gas Control 4, 546–560.

Dusseault, M.B., Gray, M.N., Nawrocki, P.A., 2000. Why oilwells leak: cement behavior and long-term consequences. In: SPE Paper 64733. SPE International Oil and Gas Conference and Exhibition, Beijing, China, November 7–10.

Gaboreau, S., Lerouge, C., Dewonck, S., Linard, Y., Bourbon, X., Fialips, C.I., Mazurier, A., Prêt, D., Bosrchenck, D., Montouillout, V., Gaucher, E.C., Claret, F., 2012. In situ interaction of cement and shotcrete with claystones in a deep disposal context. Am. J. Sci. 312, 314–356.

Gasda, S.E., Nordbotten, J.M., Celia, M.A., 2008. Determining effective wellbore permeability from a field pressure test: a numerical analysis of detection limits. Environ. Geol. 54, 1207–1215.

Gaucher, E.C., Lassin, A., Lerouge, C., Flehoc, C., Marty, N.C.M., Henry, B., Tournassat, C., Atlmann, S., Vinsot, A., Buschaert, S., Matray, J.M., Leupin, O.X., de Craen, M., 2010. CO_2 partial pressure in clayrocks: a general model. In: Birkle, P., Alvarado, I.S.T. (Eds.), Proceedings of the 13th International Conference on Water-rock Interaction Wri-13. Guanajuato, Mexico, 16–20 August, p. 2010.

Huerta, N.J., Hesse, M.A., Bryant, S.L., Strazisar, B.R., Lopano, C.L., 2013. Experimental evidence for self-limiting reactive flow through a fractured cement core: implications for time-dependent wellbore leakage. Environ. Sci. Technol. 47, 269–275.

Huerta, N.J., Hesse, M.A., Bryant, S.L., Strazisar, B.R., Lopano, C., 2016. Reactive transport of CO_2-saturated water in a cement fracture: application to wellbore leakage during geologic CO_2 storage. Int. J. Greenh. Gas Control 44, 276–289.

Jenni, A., Mäder, U., Lerouge, C., Gaboreau, S., Schwyn, B., 2014. In situ interaction between different concretes and opalinus clay. Phys. Chem. Earth Parts A/B/C 70–71, 71–83.

Jung, H.B., Um, W., 2013. Experimental study of potential wellbore cement carbonation by various phases of carbon dioxide during geologcial carbon sequestration. Appl. Geochem. 35, 161–172.

Koroleva, M., Lerouge, C., Mäder, U., Claret, F., Gaucher, E., 2011. Biogeochemical processes in a clay formation in situ experiment: part b – results from overcoring and evidence of strong buffering by the rock formation. Appl. Geochem. 26, 954–966.

Kuperschmied, N., Wild, K.M., Amann, F., Nussbaum, C., Jaeggi, D., Badertscher, N., 2015. Time-dependent fracture formation around a borehole in a clay shale. Int. J. Rock Mech. Min. 77, 105–114.

Kutchko, B.G., Strazisar, B.R., Dzombak, D.A., Lowry, G.V., Thaulow, N., 2007. Degradation of well cement by CO_2 under geologic sequestration conditions. Environ. Sci. Technol. 41, 4787–4792.

Kutchko, B.G., Strazisar, B.R., Lowry, G.V., Dzombak, D.A., Thaulow, N., 2008. Rate of CO_2 attack on hydrated class H well cement under geologic sequestration conditions. Environ. Sci. Technol. 42, 6237–6242, PMID: 18767693.

Kutchko, B.G., Strazisar, B.R., Huerta, N., Lowry, G.V., Dzombak, D.A., Thaulow, N., 2009. CO_2 reaction with hydrated class H well cement under geologic sequestration conditions: effects of fly ash admixtures. Environ. Sci. Technol. 43, 3947–3952.

Lassin, A., Marty, N.C.M., Gailhanou, H., Henry, B., Trémosa, J., Lerouge, C., Madé, B., Altmann, S., Gaucher, E.C., 2016. Equilibrium partial pressure of CO_2 in Callovian-Oxfordian argillite as a function of relative humidity: experiments and modelling. Geochim. Cosmochim. Acta, http://dx.doi.org/10.1016/j.gca.2016.04.028.

Lemmon, E.W., Huber, M.L., McLinden, M.O., 2013. NIST Standard Reference Database 23: Reference Fluid Thermodynamic and Transport Properties-REFPROP, Version 9.1. National Institute of Standards and Technology, Standard Reference Data Program, Gaithersburg.

Lerouge, C., Blessing, M., Flehoc, C., Gaucher, E.C., Henry, B., Lassin, A., Marty, N., Matray, J.M., Proust, E., Rufer, D., Tremosa, J., Vinsot, A., 2015. Dissolved CO_2 and alkane gas in clay formations. Procedia Earth Planet. Sci. 13 (2015), 88–91, 11th Applied Isotope Geochemistry Conference, AIG-11 BRGM.

Lesti, M., Tiemeyer, C., Plank, J., 2013. CO_2 stability of Portland cement based well cementing systems for use on carbon capture & storage (CCS) wells. Cem. Concr. Res. 45, 45–54.

Liteanu, E., Spiers, C., 2011. Fracture healing and transport properties of wellbore cement in the presence of supercritical CO_2. Chem. Geol. 281, 195–210.

Luquot, L., Abdoulghafour, H., Gouze, P., 2013. Hydro-dynamically controlled alteration of fractured Portland cements flowed by CO_2-rich brine. Int. J. Greenh. Gas Control 16, 167–179.

Manceau, J.C., Tremosa, J., Audigane, P., Lerouge, C., Claret, F., Lettry, Y., Fierz, T., Nussbaum, C., 2015. Well integrityassessment under temperature andpressure stresses by a 1:1 scalewellbore experiment. Water Resour. Res. 51, 6093–6109, http://dx.doi.org/10.1002/2014WR016786.

Mason, H.E., Du Frane, W.L., Walsh, S.D., Dai, Z., Charnvanichborikarn, S., Carroll, S.A., 2013. Chemical and mechanical properties of wellbore cement alteredby CO_2-rich brine using a multianalytical approach. Environ. Sci. Technol. 47, 1745–1752.

Nelson, E.B., 1990. Well Cementing. Schlumberger Educational Services, Sugarland, TX.

Parkhurst, D.L., Appelo, C.A.J., 2013. Description of Input and Examples for PHREEQC Version 3–a Computer Program for Speciation, Batch-reaction, One-dimensional Transport, and Inverse Geochemical Calculations. U.S. Geological Survey Techniques and Methods, Book 6, Chapter A43.

Pearson, F.J., Tournassat, C., Gaucher, E.C., 2011. Biogeochemical processes in a clay formation in situ experiment: part E—equilibrium controls on chemistry of pore water from the Opalinus Clay, Mont Terri Underground Research Laboratory, Switzerland. Appl. Geochem. 26, 990–1008.

Pruess, K., Oldenburg, C.M., Moridis, G.J., 1999. TOUGH2 User's Guide, Version 2.0. LBNL Report LBNL-43134.

Rimmelé, G., Barlet-Gouédard, V., Porcherie, O., Goffé, B., Brunet, F., 2008. Heterge-neous porosity distribution in portland cement exposed to CO_2-rich fluids. Cem. Concr. Res. 38, 1038–1048.

Talabani, S., Atlas, B., Al-Khatiri, M., Islam, M., 2000. An alternate approach to downhole corrosion mitigation. J. Petrol. Sci. Eng. 26, 41–48.

Vrålstad, T., Skorpa, R., Opedal, N., De Andrade, J., 2015. Effect of thermal cycling on cement sheath integrity: realistic experimental tests and simulation of resulting leakages. In: Paper SPE-178467 Presented at the SPE Thermal Well Integrity and Design Symposium Held in Banff, Alberta, Canada, 23–25 November.

Walsh, S.D., Du Frane, W.L., Mason, H.E., Carroll, S.A., 2013. Permeability of wellbore-cement fractures following degradation by carbonated brine. Rock Mech. Rock Eng. 46, 455–464.

Walsh, S.D., Mason, H.E., Wyatt, L., Du Frane, W.L., Carroll, S.A., 2014. Mechanical and hydraulic coupling in cement–caprock interfaces exposed to carbonated brine. Int. J. Greenh. Gas Control 25, 109–120.

Wersin, P., Leupin, O.X., Mettler, S., Gaucher, E.C., Mäder, U., De Cannière, P., Vinsot, A., Gäbler, H.E., Kunimaro, T., Kiho, K., Eichinger, L., 2011. Biogeochemical processes in a clay formation in situ experiment: part A—overview, experimental design and water data of an experiment in the Opalinus Clay at the Mont Terri Underground Research Laboratory, Switzerland. Appl. Geochem. 26, 931–953.

Wigand, M., Kaszuba, J.P., Carey, J.W., Hollis, W.K., 2009. Geochemical effects of CO_2 sequestration on fractured wellbore cement at the cement/caprock interface. Chem. Geol. 265, 122–133.

Xu, T., Spycher, N., Sonnenthal, E., Zheng, L., Pruess, K., 2012. TOUGHREACT User's Guide: A Simulation Program for Non-isothermal Multiphase Reactive Transport in Variably Saturated Geologic Media Version 2.0. Earth Sciences Division, Lawrence Berkeley National Laboratory, Berkeley, USA.

Zhang, M., Bachu, S., 2011. Review of integrity of existing wells in relation to CO_2 geological storage: what do we know? Int. J. Greenh. Gas Control 5, 826–840.